Antimicrobial Agents and Chemotherapy

Microscopic and Spectroscopic Analyses of Chlorhexidine Tolerance in Delftia acidovorans Biofilms

Tara Rema, John R. Lawrence, James J. Dynes, Adam P. Hitchcock and Darren R. Korber
Antimicrob. Agents Chemother. **2014, 58(10):5673. DOI: 10.1128/AAC.02984-14.**
Published Ahead of Print 14 July 2014.

AAC Journals.ASM.org

Microscopic and Spectroscopic Analyses of Chlorhexidine Tolerance in *Delftia acidovorans* Biofilms

Tara Rema,[a] John R. Lawrence,[b] James J. Dynes,[c] Adam P. Hitchcock,[d] Darren R. Korber[a]

Food and Bioproduct Sciences, University of Saskatchewan, Saskatoon, Saskatchewan, Canada[a]; Environment Canada, Saskatoon, Saskatchewan, Canada[b]; Canadian Light Source, Inc., University of Saskatchewan, Saskatoon, Saskatchewan, Canada[c]; Chemistry & Chemical Biology, McMaster University, Hamilton, Ontario, Canada[d]

The physicochemical responses of *Delftia acidovorans* biofilms exposed to the commonly used antimicrobial chlorhexidine (CHX) were examined in this study. A CHX-sensitive mutant (MIC, 1.0 μg ml^{-1}) was derived from a CHX-tolerant (MIC, 15.0 μg ml^{-1}) *D. acidovorans* parent strain using transposon mutagenesis. *D. acidovorans* mutant (MT51) and wild-type (WT15) strain biofilms were cultivated in flow cells and then treated with CHX at sub-MIC and inhibitory concentrations and examined by confocal laser scanning microscopy (CLSM), scanning transmission X-ray microscopy (STXM), and infrared (IR) spectroscopy. Specific morphological, structural, and chemical compositional differences between the CHX-treated and -untreated biofilms of both strains were observed. Apart from architectural differences, CLSM revealed a negative effect of CHX on biofilm thickness in the CHX-sensitive MT51 biofilms relative to those of the WT15 strain. STXM analyses showed that the WT15 biofilms contained two morphochemical cell variants, whereas only one type was detected in the MT51 biofilms. The cells in the MT51 biofilms bioaccumulated CHX to a similar extent as one of the cell types found in the WT15 biofilms, whereas the other cell type in the WT15 biofilms did not bioaccumulate CHX. STXM and IR spectral analyses revealed that CHX-sensitive MT51 cells accumulated the highest levels of CHX. Pretreating biofilms with EDTA promoted the accumulation of CHX in all cells. Thus, it is suggested that a subpopulation of cells that do not accumulate CHX appear to be responsible for greater CHX resistance in *D. acidovorans* WT15 biofilm in conjunction with the possible involvement of bacterial membrane stability.

Antimicrobials are extensively used in clinical, domestic, and industrial applications, resulting in their continuous release into the environment, usually via sewage effluents. The presence of these compounds in the environment has led to concerns regarding the selection of bacterial strains that have reduced susceptibilities toward various kinds of antimicrobials (1). Chlorhexidine (CHX) is a widely used broad-spectrum antimicrobial agent, and its implications for microorganisms and the environment have received various degrees of attention since its introduction (2). Chemically a cationic, hydrophobic, and lipophilic bisbiguanide ($C_{22}H_{30}Cl_2N_{10}2C_6H_{12}O_7$), CHX is an active ingredient in many disinfectants, antiseptics, and pharmaceutical preservatives used on a daily basis. CHX possesses broad antibacterial and antifungal activities. It reacts with negatively charged phosphate groups on microbial cell walls, causing membrane damage, enzyme inhibition, and leakage of cytoplasmic constituents (3). Extensive cell damage, coagulation of cytoplasmic constituents, and the precipitation of proteins and nucleic acids can be expected when high concentrations (2%) of CHX are used due to the interactions between CHX and phosphorylated cytoplasmic molecules (3, 4).

Although several microbes have been reported to survive in the presence of currently used concentrations of CHX (5–7), little is known about the underlying mechanisms for this tolerance. Resistance to biocides is often referred to as tolerance (8). Biocides usually have multiple cellular targets, and their effects are concentration dependent and often evaluated in terms of their ability to reduce the numbers of viable microorganisms. An earlier study indicated that CHX inhibits Gram-positive and Gram-negative bacteria at concentrations of 1 mg liter^{-1} and 2 to 2.5 mg liter^{-1}, respectively (9). However, the MIC values for CHX vary depending on the type of bacteria, phenotypic and genotypic status of the organism, and the environmental conditions. Tolerance levels might be much higher when microbes grow as biofilms (10, 11). Biofilms are assemblages of microorganisms that form at interfaces, surrounded by self-produced extracellular polymeric matrices, and they are typically attached to abiotic or biotic surfaces (10). The general mechanisms of antimicrobial resistance in biofilm bacteria have been described and discussed in scientific journals (10–12). However, the literature largely consists of phenomenological descriptions of CHX resistance in biofilm communities rather than examinations of the specific mechanisms involved. Some bacterial genera (i.e., *Proteus* and *Providencia*) may either be intrinsically resistant to CHX or have induced mechanisms of resistance due to phenotypic and genotypic changes (13). Penetration failure within biofilms, the permeability characteristics of the cellular outer membrane (14), CHX degradation (15), and the presence of resistance genes or plasmids have all been reported as possible causes for CHX resistance.

Developments in microscopy have enabled researchers to develop a better understanding of biofilms and to study their interactions with various antimicrobials (16–18). Microscopic techniques, such as confocal laser scanning microscopy (CLSM), transmission electron microscopy (TEM), and scanning transmission X-ray microscopy (STXM) (19), have been used singly or in combination to examine complex microbial communities and to map the extent, nature, and distribution of macromolecules in a

Received 7 April 2014 Returned for modification 3 May 2014
Accepted 5 July 2014
Published ahead of print 14 July 2014
Address correspondence to Darren R. Korber, darren.korber@usask.ca.

doi:10.1128/AAC.02984-14

biofilm (20, 21). Cell viability, cell morphology, biofilm architecture, and matrix composition can be studied in living fully hydrated systems using CLSM (21, 22). Fluorescent dyes, such as SYTO 9 and propidium iodide, can be employed in combination with CLSM to evaluate the potential for antimicrobial agents to influence membrane integrity and permeability (20). The distribution and concentration of CHX in combination with biomacromolecules (e.g., proteins, lipids, and polysaccharides) can be investigated using STXM at a spatial resolution of <30 nm in hydrated biofilm systems (20, 23). Sequences of images recorded over a span of photon energies at the core excitation edges can be converted to quantitative maps of these compounds using suitable quantitative reference spectra. STXM at the C 1s edge has been exploited in several studies for mapping major biomacromolecules in biofilms (20, 21, 24, 25). In addition, the vibrational signatures of chemical bonds in biomolecules within a biofilm with a spatial resolution of <10 μm can be obtained using synchrotron radiation-based Fourier transform infrared spectroscopy (SR-FTIR). Most of the relevant biological information can be obtained from the mid-infrared region (4,000 to 800 cm^{-1}). The infrared absorption spectra of organic molecules provide unique "fingerprints" that can be applied for identification purposes, with great reliability (26). Bacterial biofilm changes that occur during (i) adaptation to their surrounding environments, (ii) transportation, adsorption, and interaction kinetics of antimicrobial agents within the biofilms (27–29), and (iii) biofilm developmental stages (30) have also been monitored using SR-FTIR.

Delftia acidovorans, formerly known as *Comamonas acidovorans* and *Pseudomonas acidovorans*, is a Gram-negative bacillus ubiquitously found in soil and water. Previously considered to be nonpathogenic, reports of an association with *D. acidovorans* and a number of serious infections, including bacteremia, empyema, bacterial endocarditis, and ocular and urinary tract infections (31–34), have been increasing, thus establishing this organism as an emerging opportunistic pathogen. Studies on the effects of antimicrobial agents on *D. acidovorans* biofilms are very limited, and the available CHX literature has focused on either clinical isolates or dental biofilms. Thus, the effects on environmental *D. acidovorans* biofilms have never been reported.

In the present study, a combination of CLSM, STXM, and SR-FTIR was applied to evaluate the effects of sub-MIC and inhibitory levels of CHX on CHX-tolerant and -sensitive *D. acidovorans* biofilms to elucidate the intrinsic mechanisms of CHX resistance that may exist.

MATERIALS AND METHODS

Isolation, identification, mutant development, and MIC determination. The wild-type *D. acidovorans* (WT15) strain used in this study was isolated from South Saskatchewan River water biofilms during an earlier study on antimicrobial resistance (35). The isolate was identified by a 16S rRNA gene sequencing protocol described elsewhere (36). Sequencing was carried out at the National Research Council of Canada, Saskatoon, Saskatchewan, Canada. The sequence identity was confirmed using Basic Local Alignment Search Tool (BLAST) and Sequence Match of the Ribosomal Database Project (RDP), comparing the obtained sequence to species with ≥99% match. Mutants were created from the WT15 strain using the EZ-Tn*5* <KAN2> Tnp Transposome kit (Epicentre Biotechnologies, Madison, WI), according to the supplier's instructions, and screened for sensitivity to CHX. The gene disrupted by Tn*5* insertion was identified as *tolQ*, a component of the *tolQRAB* gene cluster known to be involved in outer membrane stability in many bacterial species (data not shown).

The MIC, defined as the lowest concentration of CHX sufficient to inhibit the growth of the bacteria, was determined for WT15 and selected mutants by the microdilution method (37) using different concentrations of CHX dihydrochloride (Sigma-Aldrich Co., St. Louis, MO). The mutant (MT51) selected for this study had a CHX MIC of 1.0 μg ml^{-1}, compared to an MIC of 15 μg ml^{-1} for the WT15 parent strain.

Bacterial and culture conditions. The *D. acidovorans* (WT15 and MT51) strains were grown from frozen stock cultures stored in 10% (vol/vol) glycerol at −80°C (38) on tryptic soy agar (TSA) plates and incubated overnight at room temperature (RT) (23 ± 2°C). A well-isolated colony was transferred to 50 ml of 1% (full-strength, 30 g $liter^{-1}$) tryptic soy broth (TSB) in an Erlenmeyer flask and incubated on a gyratory shaker (150 ± 5 rpm) at RT until the mid-log phase of growth was reached (at approximately 14 h). This log-phase culture was then used to inoculate the flow cells set up for the study.

Cultivation of biofilms for confocal laser scanning microscopy analysis. The multichannel flow cells for CLSM biofilm analysis were constructed as previously described (22). The flow cell apparatus was sterilized with 5.25% (wt/vol) sodium hypochlorite solution for ≥15 min and then flushed using sterile water, followed by sterile growth medium (1% TSB). The biofilms of the WT15 and MT51 strains were cultivated by injecting 0.5 ml of log-phase cells, prepared as outlined above, into each channel of the flow cell. During inoculation, the flow cells were left undisturbed for 30 min to facilitate the attachment of the cells to the flow cell surface, after which pumping of the growth medium was resumed, thereby washing out unattached cells. Growth medium (1% TSB) was continuously pumped through each flow cell channel at a bulk flow rate of 25 ml h^{-1} (0.07 cm s^{-1} laminar flow velocity) using a peristaltic pump (202U; Watson Marlow, Cornwall, United Kingdom) for 24 h. To evaluate the effect of CHX, established (24-h) biofilms were then continuously treated for another 24-h period with sterile 1% TSB supplemented with 0 (control), 10 μg ml^{-1} (sublethal), or 30 μg ml^{-1} (inhibitory) CHX.

Cultivation of biofilms for STXM analysis. The flow cells for STXM analysis were constructed as previously described (23). Briefly, a silicon nitride window (Silson Ltd., Blisworth, United Kingdom) was placed between two glass microscope slides modified to accommodate inlet and outlet tubing, sealed with silicon adhesive, and then the entire flow cell apparatus was sterilized by autoclaving.

The inoculation and growth conditions (i.e., medium and pumping) were as outlined above. The biofilm cultivation period for STXM analysis was 12 h instead of the 24 h used in the CLSM study, as STXM analysis is limited to a maximum biofilm thickness of 10 μm. The 12-h biofilms were treated for a further 12 h with sterilized medium supplemented with either 0 or 10 μg ml^{-1} CHX, after which the windows were removed from the flow cells, air-dried, and fixed to the STXM sample holder. In a separate experiment, to examine the effect of inhibitory CHX concentrations, the 12-h (cultivation period) biofilms were treated with sterilized medium supplemented with 30 μg ml^{-1} and 100 μg ml^{-1} CHX for 0.5 and 1 h. The windows were then removed from the flow cells, air-dried, and fixed to the STXM sample holder. To further study CHX accumulation over time, the 12-h biofilms on the silicon nitride windows were treated with sterilized medium supplemented with 30 μg ml^{-1} CHX and removed from the flow cells after 1 and 12 h of CHX exposure, air-dried, and fixed to the STXM sample holder.

Lastly, to investigate the effect of CHX on cell membrane-permeabilized biofilms, the WT15 biofilms were grown for 12 h using sterilized medium supplemented with 1 mM EDTA, a known membrane permeabilizer, and then continuously treated for 12 h with sterilized medium supplemented with 10 μg ml^{-1} CHX, after which the windows were removed, air-dried, and fixed to the STXM sample holder. Untreated biofilms (no CHX) were compared as a control.

Cultivation of biofilms for IR spectroscopy. The flow cell setup for IR analysis was similar to that used for STXM analysis, except that the biofilms were grown directly on IR slides (Kevley Technologies, Chesterland,

OH), with the internal reflection element as the substratum. Accordingly, the IR slide was sealed with silicone adhesive to a microscope glass slide having inlet and outlet ports. The flow cells were inoculated as described earlier, incubated under flowing conditions for 24 h, and then treated with sterilized medium supplemented with 0 (control), 10, or 30 μg ml^{-1} CHX for an additional 24 h. The IR slides with attached biofilms were then removed and air-dried prior to IR analysis.

Confocal laser scanning microscopy and data analysis. CLSM was used in conjunction with the *Bac*Light LIVE/DEAD staining kit (Molecular Probes, Life Technologies, Burlington, Ontario, Canada), i.e., SYTO 9 (live) and propidium iodide (dead), to quantify *D. acidovorans* viability in biofilms following 24-h CHX treatment, as follows. The flow cells were mounted on the stage of the confocal microscope and treated with the LIVE/DEAD stain for 5 min, in accordance with the manufacturer's instructions. Optical thin sections were collected at 1-μm intervals from the attachment surface at five randomly chosen locations in each flow cell channel using a Bio-Rad MRC-1024 LaserSharp fluorescence scanning confocal laser system (Carl Zeiss MicroImaging GmbH, Jena, Germany). Dual-channel images, corresponding to fluorescence emission in the green (excitation/emission, 488/522 nm) (SYTO 9) and red (excitation/emission, 535/617 nm) (propidium iodide) wavelengths, were acquired in either the *xy* (as indicated above) or vertical *xz* planes. Digital image analysis (NIH image software, version 1.63f; National Institutes of Health, Bethesda, MD) of the optical thin sections was then used to determine the cell viability and live/dead ratios (% fluorescence) at 48 h for both the control and CHX-treated biofilms. Biofilm thickness was measured in micrometers with the aid of a computer-controlled motorized *z* axis stepper motor, and manual focusing was done with a Nikon Microphot-FXA microscope (Nikon Corp., Tokyo, Japan) (17). The average thickness values were calculated from 5 random fields for each biofilm, with thickness values measured at 5 separate locations per field. This analysis was experimentally replicated in triplicate for a total of 75 thickness measurements per treatment.

Scanning transmission X-ray microscopy and data analysis. X-ray imaging and spectromicroscopy of the biofilms prepared as described above were carried out using STXM microscopes on beamlines 5.3.2.2 at the Advanced Light Source (ALS) (Berkeley, CA) (39) and the SM beamline 10ID-1 at the Canadian Light Source (CLS) (Saskatoon, Saskatchewan, Canada) (40). Near-edge X-ray fine structure absorption spectra (NEXAFS) were collected at the C 1s edge at a single energy or as a sequence of energies (i.e., an 80- to 100-image stack) from 280 to 320 eV. The raw transmitted signals were converted to optical densities (absorbances) using the incident flux signals measured at regions without biofilms, correcting for absorbance by the silicon nitride windows. Quantitative component maps of the major biomacromolecules (proteins, lipids, and polysaccharides) as well as CO_3^{2-}, K^+, and CHX, were derived by fitting the image sequences at each pixel to the spectra of the reference compounds that had been placed on an absolute linear absorbance scale using the singular value decomposition procedure (38). Absolute linear absorbance is the optical density (OD) per unit path length of a pure material of a defined density, where the absorbance (A), also called OD, is given by the equation $A = \mathrm{OD} = -\ln(I/\mathrm{Io})$, where I is the transmitted intensity and Io is the incident intensity, and it is established by adjusting the intensity scale of the reference spectrum to that of the computed elemental response outside the structured near-edge region (41). The lower and upper limits of the gray scale indicated in the component maps are a measure of the component thickness in nm. The reliability and methodology used to quantitatively map the major biomacromolecules in biofilm cells have been described in detail elsewhere (19, 23, 41). The reference compounds used were protein (human serum albumin), lipid (1,2-dipalmitoyl-*sn*-glycero-3-phosphocholine), polysaccharide (xanthan gum), carbonate (calcite), K (K_2CO_3 with CO_3 derived from Ca carbonate subtracted) (20, 22), and chlorhexidine dihydrochloride (CHX). The microscope energy scale was calibrated to ±0.05 eV accuracy using the Rydberg peaks of CO_2. The analysis was carried out using the aXis2000 software (http://unicorn.mcmaster.ca/aXis2000.html).

TABLE 1 Thicknesses of treated (10 and 30 μg ml^{-1} CHX) and control *D. acidovorans* WT15 and MT51 biofilms as determined using CLSM

Biofilm type (dose in μg ml^{-1})	Avg thickness (μm)[a]
WT15 control	16.3 ± 4.3 B
WT15 treated (10)	18.0 ± 6.4 B
WT15 treated (30)	16.0 ± 3.3 B,C
MT51 control	31.3 ± 9.0 A
MT51 treated (10)	13.2 ± 7.0 C,D
MT51 treated (30)	8.4 ± 3.9 D

[a] Values are the means ± standard deviations (SD) from 3 separate experiments. Values followed by the same capital letters are not significantly different at a P value of <0.05.

Infrared spectroscopy and data analysis. Air-dried 48-h CHX-treated and control biofilms were analyzed using the midinfrared spectromicroscopy (mid-IR) beamline 01B1-1 at the Canadian Light Source, Saskatoon, using a Bruker Optics IFS66v/s FTIR spectrometer and a Hyperion 2000 IR microscope. The slides were mounted on the microscope, and the area to be analyzed was focused, after which the chamber was tightly closed and flushed with nitrogen gas for ≥15 min to minimize CO_2 and water vapor interference. The instrument was operated using the following settings: reflectance mode, phase resolution of 32 cm^{-1}, scanner velocity of 40.0 KHz, and an aperture size of 12 μm by 12 μm (±3 μm). The samples were scanned over a wide spectral range, i.e., from 4,000 cm^{-1} to 800 cm^{-1}. Single-point background scans (n = 5,000) were taken on the IR slide that was free of biofilm material to establish the background noise level. The biofilm samples were scanned at 24 different points 256 times each at a resolution of 4 cm^{-1}. The reference spectrum was developed by dissolving a small quantity of CHX dihydrochloride in distilled water, followed by spreading and drying as a thin layer on the IR slide, and scanning at a single point (n = 128; resolution, 4 cm^{-1}). All the spectra were derived and analyzed using the OPUS software (Bruker Optics, Inc., Billerica, MA).

RESULTS

CLSM analysis of CHX-treated *D. acidovorans* biofilms. CLSM was used to visualize the baseline biofilm structure, thickness, and cell viability in the presence (10 and 30 μg ml^{-1}) and absence of CHX. Both the CHX-tolerant WT15 and CHX-sensitive MT51 strains attached to the glass surfaces of the flow cells and developed into biofilms within 24 h in the absence of CHX, after which they were exposed to CHX. The average thickness of the untreated MT51 biofilms after 48 h was 31.3 ± 9 μm, compared to 16.3 ± 4.3 μm for the untreated WT15 biofilms (Table 1). When the 24-h *D. acidovorans* WT15 and MT51 biofilms were treated with TSB supplemented with 10 μg ml^{-1} CHX for an additional 24 h, the mutant biofilm thickness was significantly ($P < 0.05$) reduced to 13.2 μm, whereas the wild-type biofilm increased in thickness by 2 μm. When a concentration of 30 μg ml^{-1} CHX was applied for the same exposure period, the WT15 biofilm ceased to grow, whereas the MT51 biofilm cells were virtually all detached from the glass surface and washed out.

Differences were also seen in the architecture of the CHX-treated and -untreated biofilms. Figures 1A and C show typical CLSM images of 48-h control WT15 and MT51 biofilms, respectively; the WT strain grew as spatially isolated individual microcolonies consisting of relatively densely packed cells. In accordance with this heterogeneous architecture, the thickness of the WT15 biofilm varied throughout the flow channel. In contrast, the MT51 biofilm consisted of uniformly distributed cells en-

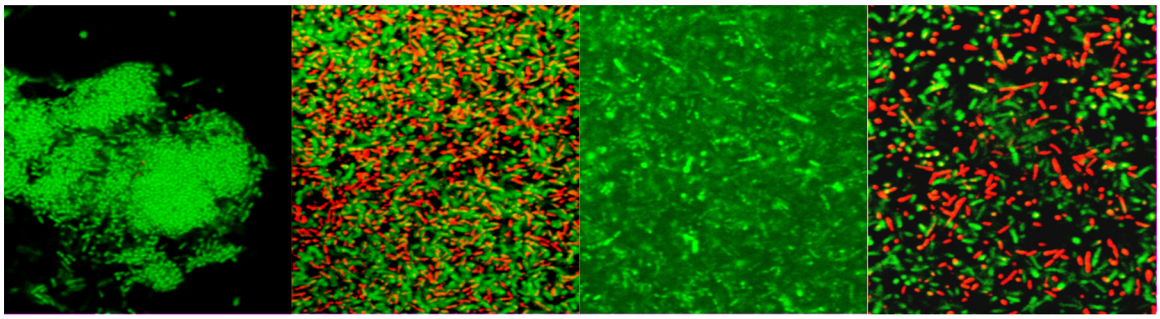

FIG 1 CLSM images obtained from the 5-μm sectioning depth of 48-h-treated (10 μg ml^{-1} CHX) and untreated WT15 and MT51 *D. acidovorans* biofilms stained with *Bac*Light LIVE/DEAD stain. The biofilms were grown for 24 h using 1% TSB and then cultivated for an additional 24 h in the presence or absence of 10 μg ml^{-1} CHX. (A) WT15 control; (B) WT15 treated; (C) MT51 control; (D) MT51 treated biofilms. Green, viable cells; red, nonviable cells.

closed within an extensive extracellular polymeric substance (EPS) matrix (31.3 ± 9.0 μm). Following 24 h of exposure to 10 μg ml^{-1} CHX, the biofilm matrices appeared similar between the two cases; the WT15 biofilms underwent a shift in their microcolony structure and became more homogenously distributed like the MT51 biofilms (Fig. 1B and D). Individual cells within the biofilm were more clearly seen after the MT51 biofilms were exposed to CHX, and they appeared to be less dense than the WT15 biofilms.

SYTO 9 and propidium iodide staining was used to determine the proportion of live and dead cells, respectively, in the WT15 and MT51 biofilms grown in the presence and absence of CHX. The vertical distribution of living cells within the first 20 μm of the biofilms after 48 h of growth is illustrated in Fig. 2. The untreated biofilms consisted of 98 to 99% viable cells throughout the vertical profile in the case of both the WT15 and MT51 biofilms. However, the mean viability of both WT15 and MT51 biofilms decreased following treatment with 10 and 30 μg ml^{-1} CHX relative to the untreated control biofilms. In the presence of 10 μg ml^{-1} CHX, the proportion of viable cells in the WT15 biofilm increased with

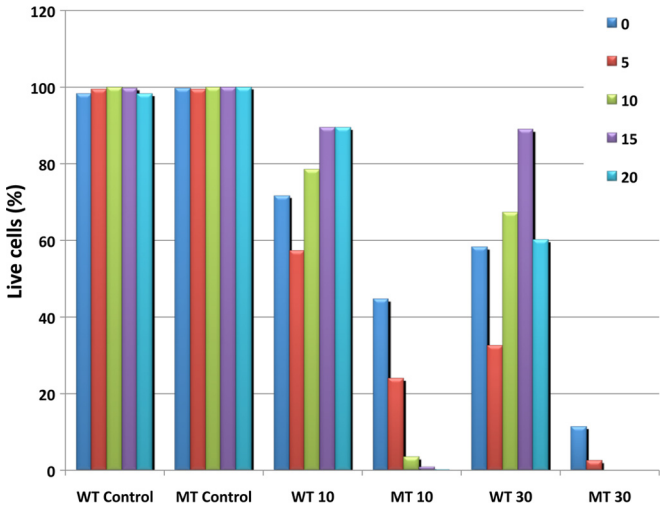

FIG 2 Viability profiles of 48-h WT15 and MT51 *D. acidovorans* biofilms grown for the previous 24 h in the presence or absence of CHX (10 and 30 μg ml^{-1}). Determinations were made by analyzing CLSM optical thin sections of *Bac*Light LIVE/DEAD-stained biofilms obtained at the 0-, 5-, 10-, 15-, and 20-μm sectioning depths (where 0 μm is the attachment surface).

distance from the attachment surface over the entire thickness examined, in agreement with an increase in overall biofilm thickness, as illustrated in Table 1. In contrast, no definite pattern was observed for the WT15 biofilms exposed to treatment with 30 μg ml^{-1} CHX. In the case of the MT51 strain, the total viable cells decreased significantly ($P < 0.05$) with depth following both 10 and 30 μg ml^{-1} CHX treatment compared to results for the MT51 control biofilm.

Soft X-ray scanning transmission microscopy. The reference spectra used to derive the quantitative component maps for CHX and the major macromolecules in *D. acidovorans* biofilms, including protein, lipids, polysaccharides, carbonate, and K, were published previously (23) and discussed in detail (20, 21, 32). STXM images were collected at 288.2 eV for the MT51 and WT15 biofilms exposed to 0 (control) and 10 μg ml^{-1} CHX for 12 h (after 12 h of initial growth without CHX) (Fig. 3). Since bacteria are roughly composed of 50% protein, this photon energy is useful for preferentially visualizing bacterial cells, as it is mainly due to the absorption of the carbonyl moiety in the peptide band [(NH_2)-C═O] of proteins (23). The optical density is indicated by the gray scale, with white and black corresponding to higher and lower thicknesses of protein, respectively. In the absence of CHX, the protein in the WT15 cells was not evenly distributed, as evidenced by the wide variation in the optical density (Fig. 3A), whereas there was no variation in the optical density of the cells/proteins in the MT51 control system, with all being white (i.e., thickest) (Fig. 3B). Exposing the WT15 biofilms to CHX resulted in some of the cells having greater amounts of protein (Fig. 3C), suggesting that there were two different cell types, as based on their response to CHX. There was no apparent change in the optical densities of the MT51 cells when exposed to CHX (Fig. 3D). Figure 4 presents the quantitative protein, lipid, and polysaccharide component maps derived from spectral fitting of 24-h-old WT15 control biofilms (obtained from the same region as for the 288.2 eV image, Fig. 3A). The gray scale shown in the component maps is a measure of the component thickness in nm, with the lower (black) and upper (white) limits of the scale shown for each component. The color-coded composite image (Fig. 4D) shows the spatial correlation of the components. No CHX signal was detected in the control biofilms. There was variation in the protein, lipid, and polysaccharide contents within the individual cells, consisting of areas with relatively high and low content.

The quantitative protein, lipid, polysaccharide, and CHX com-

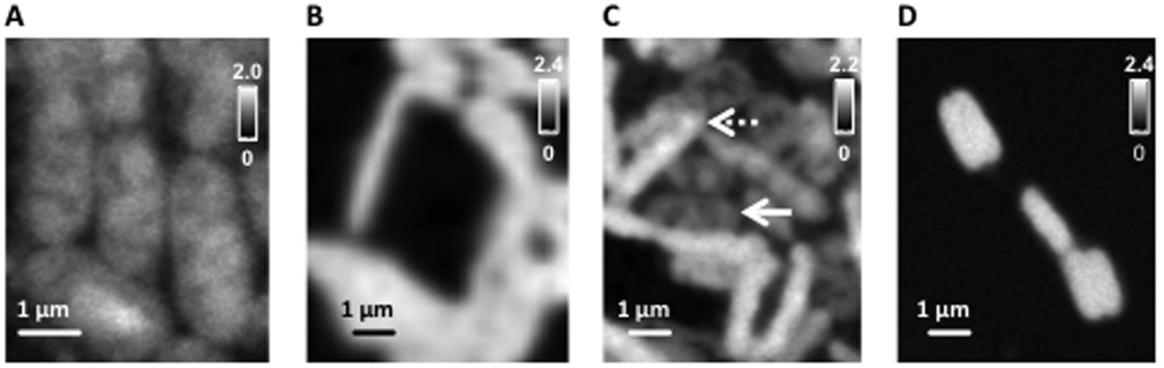

FIG 3 Optical density images (288.2 eV) represent the carbonyl of the protein in microbial cells of CHX-treated (10 μg ml^{-1} for 12 h) and control biofilms of CHX-tolerant (WT15) and CHX-sensitive (MT51) *D. acidovorans* strains after 24 h of growth. Shown are the WT15 control (A), MT51 control (B), WT15 CHX-treated (C), and MT51 CHX-treated (D) cells. The arrows indicate the two cell types observed in the biofilms as evident from the density/distribution of the protein in the cell. The gray scales indicate optical density.

ponent maps for the 24-h-old WT15 biofilms exposed to 10 μg ml^{-1} CHX for 12 h (after 12 h of initial growth without CHX) are shown in Fig. 5. From the protein component map, there were cells whose proteins were unevenly distributed, similar to that of the control biofilm (Fig. 4A and D); however, there were also cells in which the proteins were higher in concentration and were evenly distributed (Fig. 5A, arrows). This suggests that there were two cell types in these WT15 biofilms. The cells with high protein levels also had high lipid and polysaccharide content, but there was variation in their lipid and polysaccharide levels within the cells. In contrast, the lipid and polysaccharide contents were fairly evenly distributed in the cells with the low lipid and polysaccharide levels. All CHX-treated cells contained CHX, with the highest level of CHX contained by cells with high protein, lipid, and polysaccharide levels. Moreover, the spatial pattern of CHX distribution in the cells with high CHX content was similar to the lipid and polysaccharide spatial pattern.

The quantitative protein, lipid, polysaccharide, and CHX component maps for the 24-h-old MT51 biofilms exposed to 10 μg ml^{-1} CHX for 12 h (after 12 h of initial growth without CHX) are

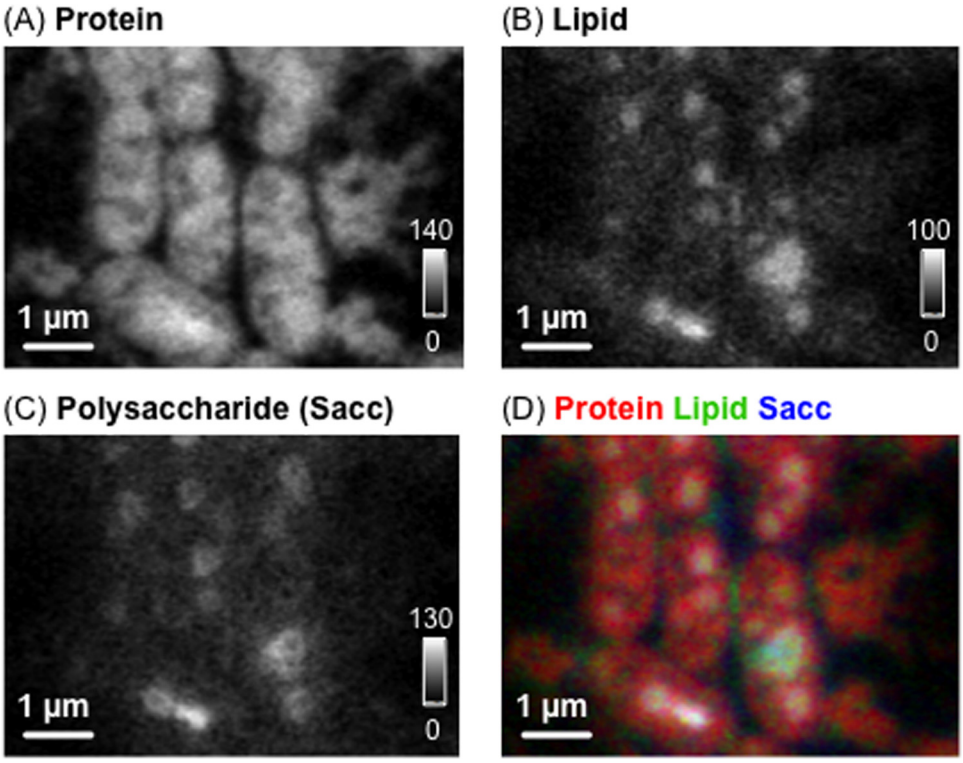

FIG 4 Component maps of 24-h CHX-tolerant (WT15) *D. acidovorans* biofilms not exposed to CHX. Shown are the (A) proteins, (B) lipids, and (C) polysaccharide (Sacc) components. (A to C) Maps derived by singular value decomposition (SVD) of an image sequence (280 to 320 eV). The gray scales indicate the effective thickness of the mapped component in nm. (D) Color-coded composites of selected component maps, where protein is red, lipid is green, and polysaccharide is blue.

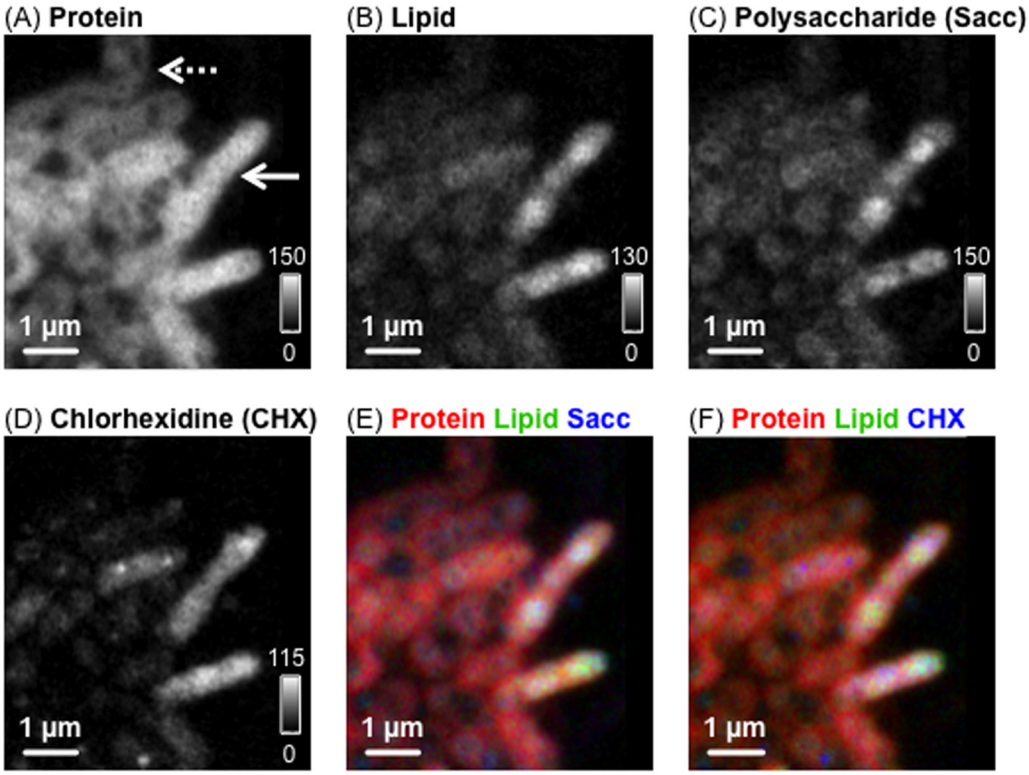

FIG 5 Component maps of 24-h CHX-tolerant (WT15) *D. acidovorans* biofilms treated with CHX (10 μg ml^{-1} for 12 h). Shown are the protein (A), lipid (B), polysaccharide (Sacc) (C), and chlorhexidine (CHX) (D) components. (A to D) Maps were derived by singular value decomposition (SVD) of an image sequence (280 to 320 eV). The gray scales indicate the effective thickness of the mapped component in nm. The color-coded composites of selected component maps are as follows: protein is red, lipid is green, and polysaccharide is blue (E), and protein is red, lipid is green, and CHX is blue (F). (A) The arrows in indicate the two cell types observed in the biofilm.

shown in Fig. 6. Only one cell type, with an even distribution of CHX, protein, and lipid, but not polysaccharide, was observed in all biofilms. The spatial distribution of CHX was different from that in the WT15 treated cells, as in this case, the pattern was similar to that of the protein and lipid, rather than of the lipid and polysaccharide, as is seen in WT15 cells. The spectral curve fitting of CHX (Fig. 6) was performed by extracting a CHX-rich region from the image sequence to include only pixels with a value of >100 nm. The numerical values extracted from the spectral fit data were 95.3 nm for protein (albumin), 55.3 nm for lipid (1,2-dipalmitoyl-*sn*-glycero-3-phosphocholine), 42.0 nm for polysaccharide (xanthan gum), and 135 nm for CHX.

The levels of CHX in the WT15 and MT51 biofilm cells treated with 10 μg ml^{-1} CHX were then compared (Fig. 5 and 6), and the WT15 cells accumulated CHX to a maximum thickness value of 115 nm, whereas the CHX-exposed MT51 cells accumulated CHX to a thickness of almost twice this value. This finding is further supported by the concentration values calculated on a per-pixel basis, as presented in Table 2, in which the MT biofilms treated with 10 μg ml^{-1} CHX accumulated five times (94.1 ± 58.3 nm) more CHX than the WT biofilms treated with 10 μg ml^{-1} CHX.

The effect of higher concentrations of CHX was studied for only the CHX-tolerant *D. acidovorans* WT15 biofilms by exposing 12-h-old WT15 biofilms to 30 and 100 μg ml^{-1} CHX for 30 and 60 min. In agreement with results obtained at the lower concentration of 10 μg ml^{-1}, two different cell variants were seen at both CHX concentrations, as well as after both exposure times. However, the majority of the cells appeared lighter in the biofilms treated with 100 μg ml^{-1} CHX (Fig. 7) than those treated with 30 μg ml^{-1} for 1 h.

Based on the above results, the effects of short (1-h) and long (12-h) CHX (30 μg ml^{-1}) exposure times were evaluated on both 12-h WT15 and MT51 biofilms. Figure 8 shows a time-dependent effect, wherein the MT51 cells accumulated more CHX over time than the CHX-tolerant WT15 cells. In comparison, CHX intensity (blue color) was less in the CHX-tolerant cells even after 12 h of exposure. This observation is further substantiated in Table 2, which quantifies the differences in CHX accumulation between the CHX-sensitive and CHX-tolerant cells exposed to above-MIC (30 μg ml^{-1}) CHX concentrations at both time intervals. Interestingly, both cell variants, described earlier, were seen in 1-h-treated WT15 and MT51 biofilms, but only the dark/dense cells were seen after long-term exposure (12 h) to CHX. The 1-h STXM images were further examined in detail and showed that the denser cells had higher levels of CHX than the lighter cells within the same biofilm for both strains (Fig. 9 and Table 3). There was not much difference in CHX concentrations among the light cells in both cases, but the darker cells within the MT51 CHX-treated biofilms had nearly twice as much CHX as their WT counterparts (Table 3). There was variation in the concentrations of other macromolecules as well between the dark and light cells in both the WT15 and MT51 biofilms (Table 3), with denser cells containing primarily more protein, followed by lipid and polysaccharide. The spatial distribution of CHX in the cells exposed for 1 h (Fig. 8)

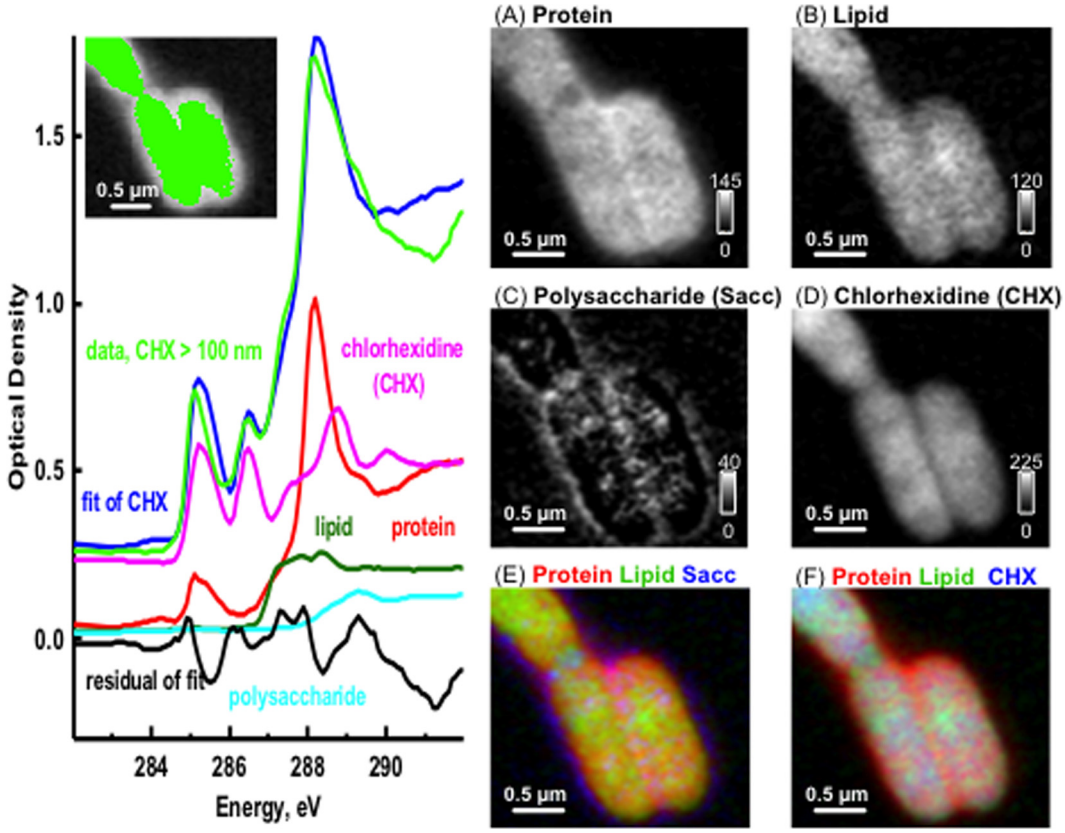

FIG 6 Component maps of 24-h CHX-sensitive (MT51) *D. acidovorans* biofilms treated with CHX (10 μg ml^{-1} for 12 h). Shown are the protein (A), lipid (B), polysaccharide (Sacc) (C), and chlorhexidine (CHX) (D) components. (A to D) Maps were derived by singular value decomposition (SVD) of an image sequence (280 to 320 eV). The color-coded composites of selected component maps are as follows: protein is red, lipid is green, and polysaccharide is blue (E), and protein is red, lipid is green, and CHX is blue (F). The gray scales indicate the effective thickness of the mapped component in nm. The curve fit to the spectrum extracted from the CHX component map with pixels having values >100 nm is also shown.

indicated that CHX was initially associated with the lipid component of the cells; however, this effect was difficult to confirm with increasing CHX exposure time, especially for the MT51 biofilms.

To further investigate the effects of CHX accumulation, the WT15 biofilms were first exposed to the membrane permeabilizing agent EDTA before exposure to 10 μg ml^{-1} CHX. Figures 10 and 11 show the component maps of the WT15 biofilm cells exposed to EDTA only and EDTA followed by CHX treatment. As shown in Table 2, treatment with EDTA promoted the bioaccumulation of CHX (almost double) in the WT15 biofilms (36.5 ± 34.8 nm per pixel) compared to the WT15 biofilms treated with CHX only (17.4 ± 19.6 nm per pixel). Furthermore, only one type, the darker cells that accumulated CHX in our earlier studies, was found to be present in the EDTA-treated biofilms (Fig. 11).

TABLE 2 Average thickness values of CHX in WT15 and MT51 CHX-treated biofilms as determined from STXM images[a]

Biofilm (dose in μg ml^{-1}, time in h)	CHX (avg ± SD) (nm per pixel)
WT15 (10, 12)	17.4 ± 19.6
MT51 (10, 12)	94.1 ± 58.3
EDTA-exposed WT15 (10, 12)	36.5 ± 34.8
WT15 (30, 1)	17.2 ± 21.2
MT51 (30, 1)	58.9 ± 43.3
WT15 (30, 12)	73.2 ± 42.3
MT51 (30, 12)	101.0 ± 52.5

[a] All treatments were carried out on 12-h established biofilms.

Infrared spectroscopy. Specific IR absorption patterns can be attributed to particular types of covalent bonds, and any modifications of these bonds by the local environment can be detected in the details of the IR spectra. Accordingly, the vibrational signa-

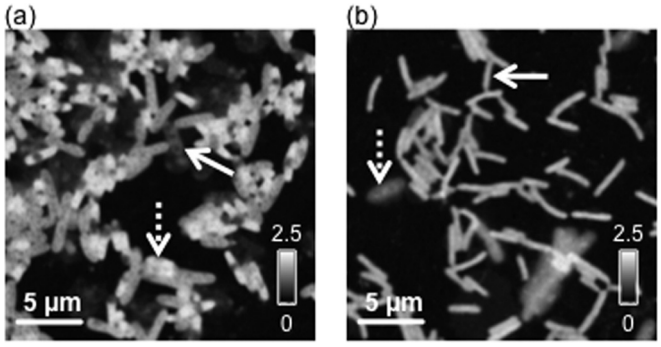

FIG 7 Optical density images (288.2 eV, represents the carbonyl of the protein in microbial cells) of CHX-tolerant (WT15) *D. acidovorans* biofilms grown for 12 h before treatment with 30 μg ml^{-1} (a) and 100 μg ml^{-1} (b) CHX for 1 h. The arrows indicate the two cell types observed in the biofilm.

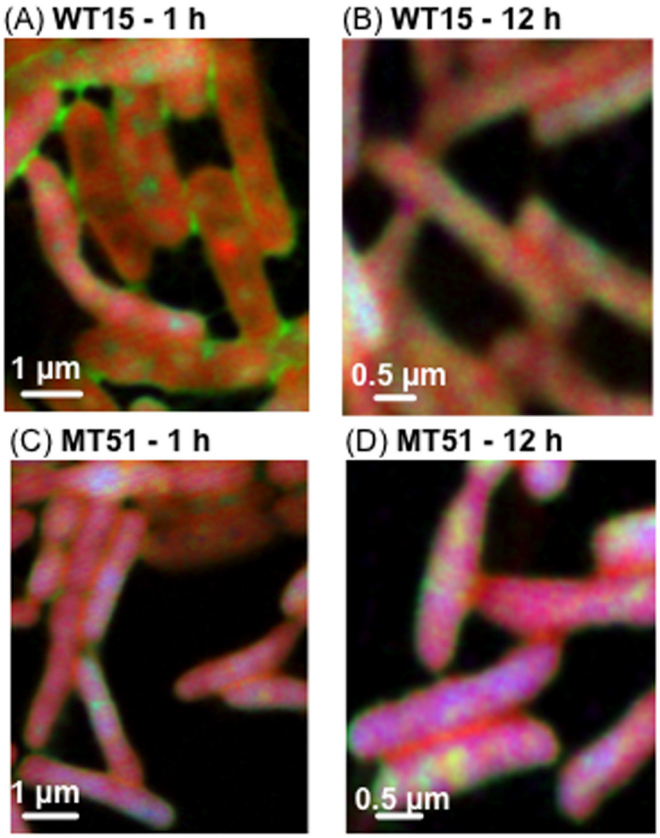

FIG 8 Color-coded composites (protein, red; lipid, green; CHX, blue) of CHX-tolerant (WT15) and CHX-sensitive (MT51) *D. acidovorans* biofilms grown for 12 h before treatment with 30 μg ml^{-1} CHX for 1 h (A and C) and 12 h (B and D), respectively.

tures of organic molecules in microbial biofilms can be measured using IR spectromicroscopy. The main absorption bands of the biofilms correlating with the experimental conditions employed in this study are plotted in Fig. 12A, with the IR spectrum of the CHX standard provided for reference. The subset panel of IR spectra reveals a peak at around 1,492 cm^{-1}, which is attributed to the chlorophenol groups of CHX (27). Two peaks at the 3,400-cm^{-1} region were also seen in the CHX IR spectrum and were attributed to μ_{as} and μ_{as}-NH, which is also suggestive of CHX (42). Peaks were also observed at 1,650, 1,600, 1,550, and 1,500 cm^{-1}, which can be attributed to the C═C stretching of the aromatic moiety of CHX (42). The peak at 1,492 cm^{-1}, enlarged in Fig. 12B, was very prominent in the CHX-sensitive MT51 biofilms treated with 10 and 30 μg ml^{-1} CHX, with the peak area being larger in biofilms receiving the 30-μg ml^{-1} treatment. In contrast, the CHX diagnostic peak at 1,492 cm^{-1} was absent in the control biofilms without CHX.

DISCUSSION

An association of *Delftia* spp. with antibiotic resistance phenomena has been referenced in the literature but is very limited overall (43–45). To our knowledge, this is the first report of *D. acidovorans* tolerance to a broad-spectrum biocide, such as CHX. Several strains of *D. acidovorans* (as *C. acidovorans*) isolated from clinical specimens have been found to be resistant to various groups of antibiotics, such as β-lactams, aminoglycosides, and quinolones (43). Chotikanatis et al. (44) summarized the previously reported antibiotic susceptibilities of *D. acidovorans* and concluded that it was resistant to gentamicin in all cases, resistant to all aminoglycosides in some cases, and generally susceptible to cephalosporins, piperacillin, aztreonam, carbapenems, quinolones, and trimethoprim-sulfamethoxazole. A positive correlation between *D. acidovorans* (as *C. acidovorans*) and residual chlorine was found in contaminated dental water units, indicating a strong resistance of this bacterium to chlorine (45). Additionally, a *D. acidovorans* strain isolated from a wastewater treatment facility was found to carry class 3 integrons, genetic elements commonly associated with antibiotic resistance genes. This finding added a new role for this group of organisms in the acquisition of resistance genes from antibiotic-resistant microbes in the environment (46).

The MICs for CHX have been tested for many bacterial species, and the range of tolerance is very large and dependent on factors such as the type of bacteria (Gram-positive or Gram-negative), method, or medium used. In a recent study (47), CHX exhibited the greatest variability when 272 *Enterococcus* strains were tested for sensitivity to biocides of different classes (quaternary ammonium compounds, a bisphenol, a biguanide, and copper sulfate), with MICs ranging from 2.5 to 2,500 mg ml^{-1}. Similarly, the MICs of CHX for 52 strains of subgingival plaque (biofilm) bacteria ranged from 8 to 500 μg ml^{-1} (48), whereas for methicillin-resistant *Staphylococcus aureus* isolates collected over 15 years, the MIC range was found to be 0.5 to 16 μg ml^{-1} (49). The MICs of four common human pathogens, *Escherichia coli*, *Klebsiella pneumoniae*, *Pseudomonas aeruginosa*, and *Staphylococcus epidermidis*, were 0.008, 0.0625, 0.125, and 0.002 μg ml^{-1}, respectively (50), and the MICs varied between 1 and 20 μg ml^{-1} for various Gram-positive and Gram-negative oral bacteria examined (28). Based on a comparison of the chlorhexidine MIC for *D. acidovorans* WT15 (15 μg ml^{-1}) with the MICs from other reported studies, WT15 can be considered "tolerant" to CHX.

While both the *D. acidovorans* WT15 and MT51 strains used in this study were demonstrated to form biofilms, the MT strain formed thicker biofilms than did the WT in the absence of CHX. The biofilm structure, in terms of cell distribution and density, was also different between the WT15 and MT51 strains (Fig. 1). The reason for this difference may be related to the fitness costs associated with CHX tolerance as a result of the Tn*5* mutation. Previous studies have demonstrated that the cost associated with chromosomal resistance will vary profoundly depending on the growth and experimental conditions used (51). The relative fitness of susceptible and resistant bacteria is measured by their reproductive success during *in vitro* culture. Many studies have reported that resistance commonly creates a fitness burden (51, 52); however, resistant mutants with no measurable costs or those with a slight advantage over the wild type have also been observed (53, 54), which is in agreement with our observations. However, in the presence of 10 μg ml^{-1} CHX, the biomass of the WT15 biofilms increased over a 24-h period, whereas there was an apparent cessation of biofilm development in the CHX-treated MT51 biofilms compared to that in their untreated counterparts. It is also possible that the exposure of MT51 cells to CHX might result in the dispersal of biomass, contributing to an apparent reduction in the thickness of MT51 biofilms. Such stimulation of biofilm development, as seen in the WT15 biofilm in the presence of sub-MICs of CHX, has been reported (3). In addition to the change in overall

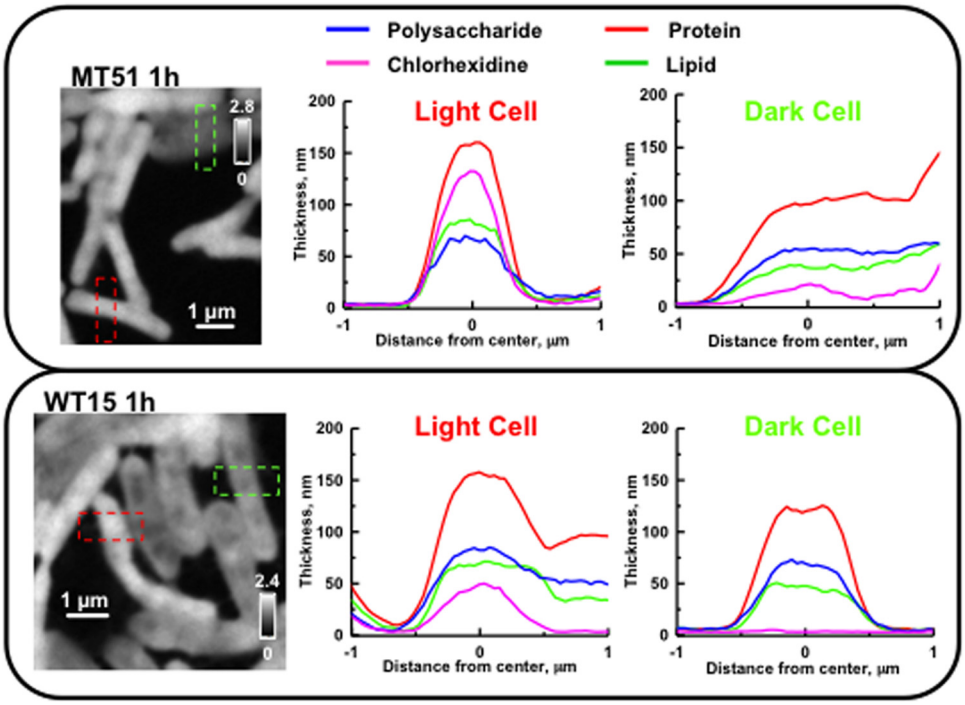

FIG 9 Intensity profiles extracted from a section of the dark and light microbial cells from the protein (red), lipid (green), polysaccharide (blue), and CHX (pink) component maps from Fig. 8 of the *D. acidovorans* WT15 and MT51 biofilms grown for 12 h before treatment with 30 μg ml^{-1} CHX for 1 h. The figures are 288.2 eV transmission images. The red and green rectangles show the area from which the profiles for the dark and light cells, respectively, were taken. The gray scales indicate optical density.

biofilm thickness observed in our study, the form and arrangement of the microcolonies in both types of biofilms became altered upon exposure to CHX. The cells in the control WT15 biofilms were arranged in very close association with each other, but upon exposure to CHX, these distinct microcolonies ceased to be evident. Hope and Wilson (3) observed biofilm contraction when 0.2% CHX was used on plaque biofilms, attributing this to ionic interactions between the negatively charged EPS matrix and the positively charged CHX molecules. They reported that these interactions changed the EPS solubility, hydrophobicity, and net charge of the matrix, thus reducing the repulsive forces between the charged moieties and allowing the biofilm matrix to contract. However, at 0.05% CHX exposure, the contraction was nonsignificant and nonuniform; hence, they concluded that biofilm contraction may be related to the concentration of CHX as well.

Since CHX effects include bacterial membrane damage (14, 18, 55), its bactericidal action can be measured using the *Bac*Light LIVE/DEAD stain (3, 20, 56, 57), which is sensitive to the permeability of the cytoplasmic membrane. Upon CHX treatment, the percentage of viable cells, based on maintaining selective membrane permeability, decreased in both the WT15 and MT51 biofilms (Fig. 2) to various degrees. The proportion of viable cells in the WT15 biofilm increased in the presence of 10 μg ml^{-1} CHX from the base of the biofilm (the attachment surface) to biomass located farther away from the attachment surface (and closest to the bulk liquid phase containing CHX). This is in agreement with an increase in biofilm thickness in the presence of CHX (Table 1). In contrast to the WT15 biofilms, a gradual loss of green fluorescence, indicative of a reduction of "living cells," was observed beginning at the biofilm-liquid interface in MT51 biofilms exposed to CHX. MT51 cells in direct contact with CHX were affected by the biocide to a greater extent than were the cells located deep within the biofilm matrix. These affected cells may have subsequently become detached from the biofilm base, an occurrence consistent with the observed reduction in biofilm thickness in the MT51 biofilms upon CHX treatment. These results are also in agreement with those of other studies (57–59) in which similar patterns of viability were observed in biofilm cells exposed to CHX. However, we did not see a complete eradication of the biofilms at either concentration of CHX (10 μg ml^{-1} or 30 μg ml^{-1}) used in this study. Interestingly, low numbers of MT51 cells continued to persist even at 30 μg ml^{-1}, a value 30× the MIC for planktonic cells (1 μg ml^{-1}), which is in agreement with the paradigm that biofilm growth renders cells 10 to 1,000 times more resistant than their planktonic counterparts (10, 11).

Confocal microscopy demonstrated the effect of CHX on the MT51 and WT15 biofilms; however, there was a need to map the spatial distribution and uptake of CHX to understand the differ-

TABLE 3 Thickness values of major macromolecules of the two cell types of 12-h established WT15 and MT51 biofilms exposed to 30 μg ml^{-1} CHX for 1 h, as determined from STXM images

Cell type	Thickness value (avg ± SD) (nm) of:			
	Protein	Lipid	Saccharide	CHX
WT15 dense	148.0 ± 19.3	69.7 ± 13.6	75.2 ± 18.0	45.5 ± 14.2
WT15 light	111.0 ± 20.2	45.1 ± 12.6	62.2 ± 15.0	6.9 ± 7.3
MT51 dense	141.0 ± 28.9	72.2 ± 20.4	61.4 ± 13.6	107.0 ± 30.9
MT51 light	95.5 ± 15.9	38.4 ± 9.3	52.3 ± 9.6	15.0 ± 8.6

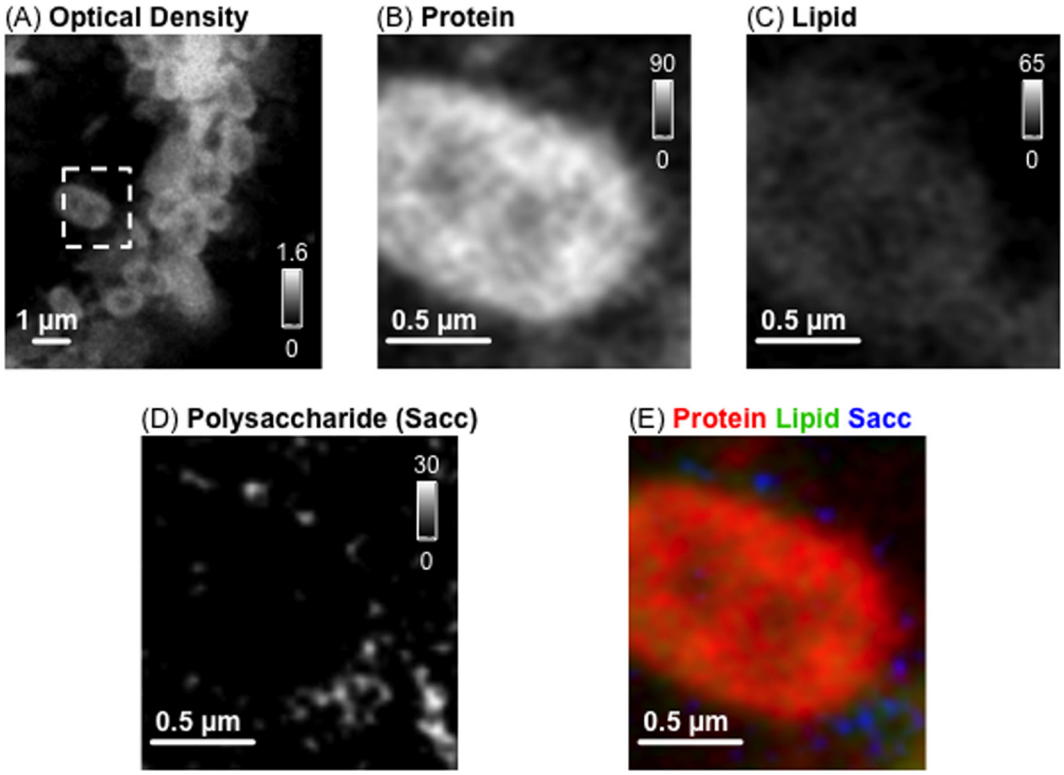

FIG 10 CHX-tolerant (WT15) *D. acidovorans* biofilms treated with 1 mM EDTA for 24 h. (A) Optical density (OD) image (288.2 eV). The gray scale indicates OD. The white dashed rectangle shows the microbial cell studied in detail. Shown are the component maps of the microbial cell protein (B), lipid (C), and polysaccharide (Sacc) (D), as well as a color-coded composite (E) of the selected component maps (protein, red; lipid, green; polysaccharide, blue). (B to D) Maps were derived by singular value decomposition (SVD) of an image sequence (280 to 320 eV). The gray scale indicates the effective thickness of the mapped component in nm. EDTA was not detected in or near the microbial cell.

ences in CHX tolerance in these two strains. Dynes et al. (23) were the first to observe the bioaccumulation of CHX in lipid-rich regions of diatoms and bacteria using STXM to study CHX-exposed river biofilms. In the present study, using STXM, the bioaccumulation of CHX was also seen in the *D. acidovorans* WT15 and MT51 biofilms, although to different extents. A significant question arises as to whether all cells in the WT15 biofilm exhibited the same level of tolerance or whether there was a subpopulation that existed as "persister" cells (12, 60) and were able to tolerate CHX. We thus suggest that the *Delftia* WT15 biofilms contain two populations (as shown in Fig. 3, 7, and 9): those that apparently do not, or only slowly, take up CHX (light cells), and those that do (dark cells), with the light cells being responsible for persistence and tolerance within the WT15 biofilms. STXM mapping results showed that CHX was distributed throughout the cell and was not linked to any particular cellular macromolecule or region. As well, the MT51 biofilm cells accumulated five times the amount of CHX as did the WT15 cells, in agreement with their increased sensitivity to CHX (Table 2). When the WT15 biofilms were exposed to higher CHX concentrations (30 μg ml^{-1} and 100 μg ml^{-1}), the number of dark cells increased accordingly. The apparent absence of light cells in the WT15 biofilms exposed to 100 μg ml^{-1} CHX indicates that intrinsic CHX tolerance tends to decrease at CHX concentrations of >30 μg ml^{-1}. Temporal analysis of biofilm cells treated with 30 μg ml^{-1} CHX also revealed that the MT51 cells accumulated more CHX than those of the WT15 strain over a 1-h period, indicating an immediate effect of CHX on the sensitive cells. Interestingly, an examination of the biofilm cells exposed to 30 μg ml^{-1} CHX for 1 h revealed the association of CHX with cellular lipids (Fig. 8), whereas at a lower CHX concentration (10 μg ml^{-1}), no association of CHX with any particular cellular component was established (Fig. 5). This finding is consistent with other reported observations (23, 61, 62) in which associations between CHX and lipids were made. This is also consistent with the fact that CHX is a positively charged hydrophobic and lipophilic molecule that interacts with negatively charged lipopolysaccharide molecules of the bacterial outer membrane before being able to enter the cell.

Our observations of the presence of two different kinds of cells within the CHX-exposed WT biofilms are supported by a similar work (63) in which an energy-dispersive analysis of X ray (EDAX) mapping revealed differences in CHX uptake between CHX-sensitive and -resistant isolates of *Pseudomonas stutzeri*. In this work, X-ray fluorescence signals of chloride (Cl) increased with time and were evenly distributed throughout the cell in a CHX-treated sensitive strain. The CHX-resistant isolates were less electron dense, and the chlorine signal increased from 30 to 60 min of treatment. Similarly, time of flight secondary-ion mass spectrometry (TOF-SIMS) analysis was also able to distinguish between the living and dead cells of *Candida albicans* biofilms that were treated with chlorhexidine digluconate (64). The dead cells did not contain high levels of intracellular potassium compared to the living ones, which is indicative of a disrupted membrane. Furthermore, the chlorhexidine digluconate intensity in the dead cells was found to

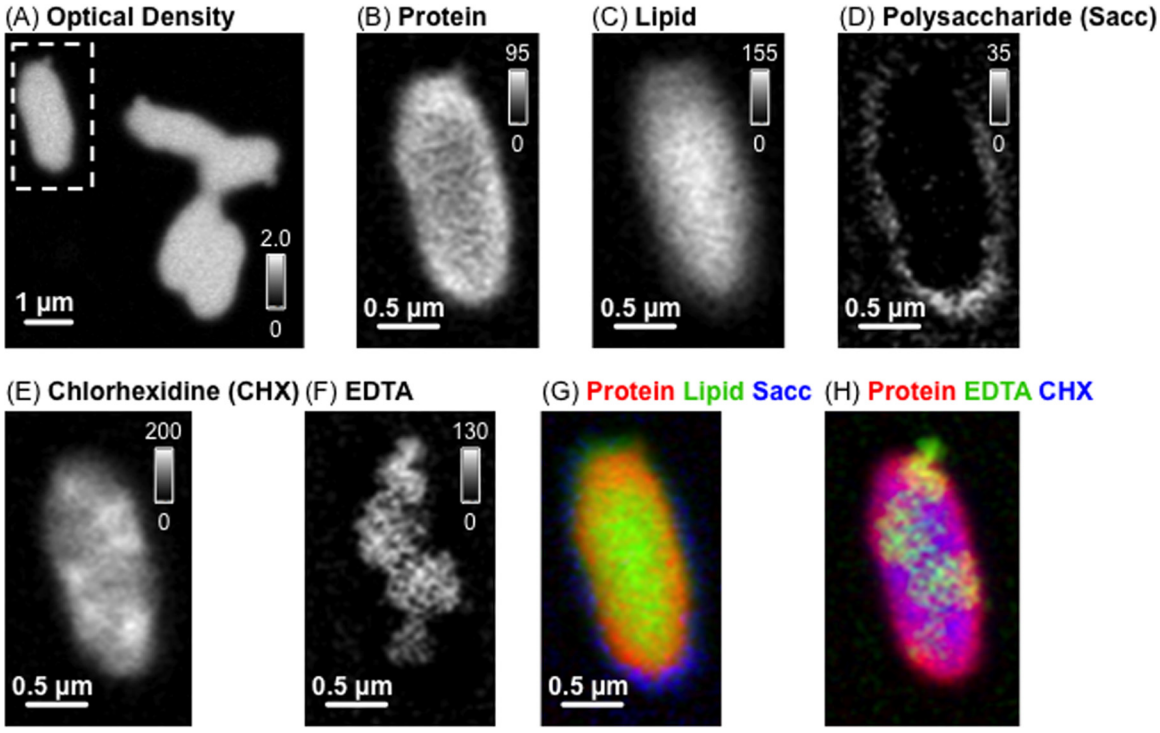

FIG 11 CHX-tolerant (WT15) *D. acidovorans* biofilms treated with 1 mM EDTA and 10 μg ml^{-1} CHX. (A) Optical density (OD) image (288.2 eV). The gray scale indicates OD. The white dashed rectangle shows the microbial cell studied in detail. Shown are the component maps of the microbial cell protein (B), lipid (C), polysaccharide (Sacc) (D), CHX (E), and EDTA (F). (B to D) Maps were derived by singular value decomposition (SVD) of an image sequence (280 to 320 eV). The gray scale indicates the effective thickness of the mapped component in nm. The color-coded composites of selected component maps are as follows: protein is red, lipid is green, and polysaccharide is blue (G), and protein is red, EDTA is green, and CHX is blue (H).

be higher than that in the surrounding medium, indicating that chlorhexidine digluconate bound preferentially to the cellular components of the *C. albicans* biofilms. Transmission electron microscopic images of *P. aeruginosa* cells treated with 10 μg ml^{-1} CHX also revealed two cell types that correlated with a sensitive and a surviving cell type (65) based on the appearance of the cell envelope.

In the present study, EDTA was shown to promote the bioaccumulation of CHX in CHX-tolerant biofilms, as CHX was mapped in all of the EDTA-treated biofilm cells (wherein all cells were of the dark morphotype), which was not the case observed when the biofilms were treated with CHX alone. This further strengthens our CLSM findings that the bacterial membrane plays a key role in *Delftia* CHX tolerance. EDTA is well known to have a significant effect on the outer membrane permeability of Gram-negative bacteria (66).

IR spectroscopy has been used to evaluate the bulk chemical changes taking place within microbial biofilms (27, 30). In our study, the results from the IR spectroscopic analysis were in agreement with our STXM results, as the diagnostic IR CHX peak at 1,492 cm^{-1} was seen in all CHX-treated biofilms but more prominently in the MT51 biofilm, particularly at high CHX concentrations (30 μg ml^{-1}). This is consistent with the observed increased accumulation of CHX in the CHX-sensitive MT51 cells detected with STXM. Since these peaks were highly comparable with those of the CHX standard, we may further conclude that CHX does not appear to be modified or degraded within *D. acidovorans* biofilms. CHX degradation studies previously conducted in our laboratory using ^{14}C-radiolabeled CHX and liquid scintillation spectrometry demonstrated that *D. acidovorans* (WT15) cannot mineralize CHX (data not shown), although CHX degradation by several other bacterial species is known to occur (15).

CHX is a clinically useful and important antibacterial agent; however, some Gram-negative bacteria appear to be highly resistant to CHX by a mechanism that is not yet fully understood. *Delftia acidovorans* biofilms provided an ideal model system for integrating analyses of CLSM, STXM, and IR data to gain insights into bacterial interactions with CHX at the micro- to nanoscales of resolution. While there were differences in the growth responses of the biofilms exposed to CHX, it was significant that the biofilm mode of growth elevated the tolerance levels (compared to the planktonic MIC values) of both the CHX-tolerant and CHX-sensitive strains of *D. acidovorans*. It thus appeared that even long-term exposure to CHX was not sufficient to completely eradicate the *D. acidovorans* biofilms of either strain. STXM allowed quantitative and high-resolution (~30 nm) *in situ* mapping of the spatial distribution of CHX in cells and revealed a differential uptake of CHX in *D. acidovorans* WT15 and MT51. The disruption of the membrane protein *tolQ* gene, along with the differential intake of CHX by these strains and the increased intake of CHX in the presence of the membrane permeabilizing agent EDTA, indicates the potential role of the cell membrane in CHX resistance. Although the microscopy/spectroscopy techniques used in this study can be employed as useful tools for studying these phenomena, more detailed molecular characterizations of the role of the

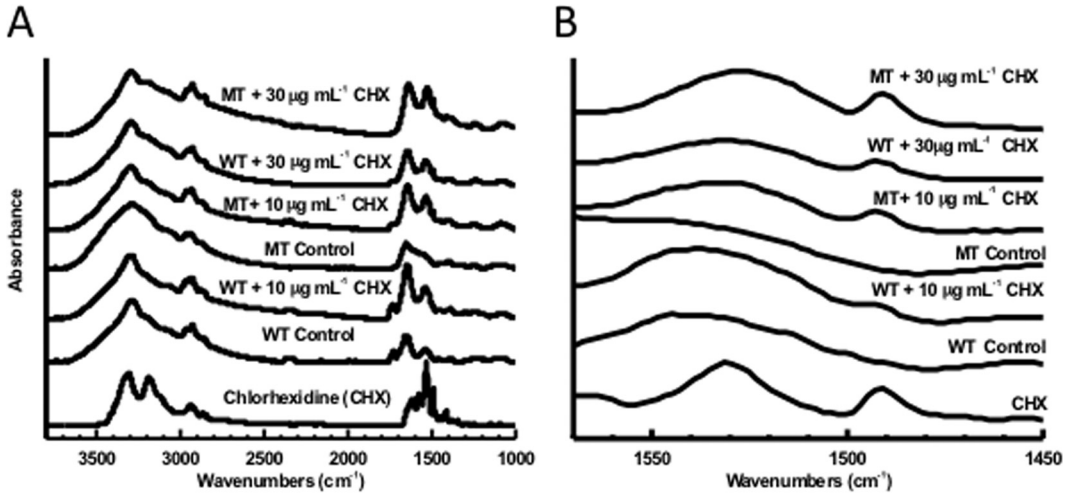

FIG 12 IR spectra obtained for *D. acidovorans* WT15 and MT51 biofilms not exposed to CHX for 48 h and CHX-treated *D. acidovorans* WT15 and MT51 biofilms (10 and 30 μg ml^{-1} for 24 h). (A) 1,000 to 4,000 cm^{-1} and (B) expansion of panel A from 1,450 to 1,600 cm^{-1}. The WT15 and MT51 control biofilms were multiplied by 5, and the CHX-treated biofilms were multiplied by 2.

tolQ gene in CHX resistance in these strains will further provide insights into the actual mechanism of CHX resistance.

ACKNOWLEDGMENTS

This work was supported by the Advanced Food and Materials Network (AFMNet), Environment Canada, Health Canada, the Canada Research Chair program (APH), and the Natural Sciences and Engineering Research Council (NSERC) of Canada. STXM measurements were performed at beamline 10ID1 at the CLS, which is supported by the NSERC, CIHR, NRC, the Province of Saskatchewan, WEDC, and the University of Saskatchewan, and at the STXM on beamline (BL) 5.3.2.2 at the ALS, which is supported by the Director, Office of Energy Research, Office of Basic Energy Sciences, Materials Sciences Division of the U.S. Department of Energy under contract DE-AC02-05CH11231.

REFERENCES

1. **Fraise AP.** 2002. Biocide abuse and antimicrobial resistance–a cause for concern? J. Antimicrob. Chemother. **49:**11–12. http://dx.doi.org/10.1093/jac/49.1.11.
2. **Lawrence JR, Zhu B, Swerhone GDW, Topp E, Roy J, Wassenaar LI, Rema T, Korber DR.** 2008. Community-level assessment of the effects of the broad-spectrum antimicrobial chlorhexidine on the outcome of river microbial biofilm development. Appl. Environ. Microbiol. **74:**3541–3550. http://dx.doi.org/10.1128/AEM.02879-07.
3. **Hope CK, Wilson M.** 2004. Analysis of the effects of chlorhexidine on oral biofilm vitality and structure based on viability profiling and an indicator of membrane integrity. Antimicrob. Agents Chemother. **48:**1461–1468. http://dx.doi.org/10.1128/AAC.48.5.1461-1468.2004.
4. **Mohammadi Z, Abbott PV.** 2009. The properties and applications of chlorhexidine in endodontics. Int. Endod. J. **42:**288–302. http://dx.doi.org/10.1111/j.1365-2591.2008.01540.x.
5. **Brooks SE, Walczak MA, Hameed R, Coonan P.** 2002. Chlorhexidine resistance in antibiotic-resistant bacteria isolated from the surfaces of dispensers of soap containing chlorhexidine. Infect. Control Hosp. Epidemiol. **23:**692–695. http://dx.doi.org/10.1086/501996.
6. **Marrie TJ, Costerton JW.** 1981. Prolonged survival of *Serratia marcescens* in chlorhexidine. Appl. Environ. Microbiol. **42:**1093–1102.
7. **Stickler DJ, Clayton CL, Chawla JC.** 1987. The resistance of urinary tract pathogens to chlorhexidine bladder washouts. J. Hosp. Infect. **10:**28–39. http://dx.doi.org/10.1016/0195-6701(87)90029-6.
8. **Favero MS.** 2002. Products containing biocides: perceptions and realities. Symp. Ser. Soc. Appl. Microbiol. **92:**72S–77S. http://dx.doi.org/10.1046/j.1365-2672.92.5s1.9.x.
9. **Russell AD, Day MJ.** 1993. Antibacterial activity of chlorhexidine. J. Hosp. Infect. **25:**229–238. http://dx.doi.org/10.1016/0195-6701(93)90109-D.
10. **Høiby N, Bjarnsholt T, Givskov M, Molin S, Ciofu O.** 2010. Antibiotic resistance of bacterial biofilms. Int. J. Antimicrob. Agents **35:**322–332. http://dx.doi.org/10.1016/j.ijantimicag.2009.12.011.
11. **Mah TF, O'Toole GA.** 2001. Mechanisms of biofilm resistance to antimicrobial agents. Trends Microbiol. **9:**34–39. http://dx.doi.org/10.1016/S0966-842X(00)01913-2.
12. **Lewis K.** 2001. Riddle of biofilm resistance. Antimicrob. Agents Chemother. **45:**999–1007. http://dx.doi.org/10.1128/AAC.45.4.999-1007.2001.
13. **Russell AD.** 1995. Mechanisms of bacterial resistance to biocides. Int. Biodeterior. Biodegr. **36:**247–265. http://dx.doi.org/10.1016/0964-8305(95)00056-9.
14. **Gilbert P, Moore LE.** 2005. Cationic antiseptics: diversity of action under a common epithet. J. Appl. Microbiol. **99:**703–715. http://dx.doi.org/10.1111/j.1365-2672.2005.02664.x.
15. **Tanaka T, Murayama S, Tuda N, Nishiyama M, Nakagawa K, Matsuo Y, Isohama Y, Kido Y.** 2005. Microbial degradation of disinfectants. A new chlorhexidine degradation intermediate (CHDI), CHDI-C, produced by *Pseudomonas* sp. strain no. A-3. J. Health Sci. **51:**357–361. http://dx.doi.org/10.1248/jhs.51.357.
16. **Mangalappalli-Illathu AK, Korber DR.** 2006. Adaptive resistance and differential protein expression of *Salmonella enterica* serovar Enteritidis biofilms exposed to benzalkonium chloride. Antimicrob. Agents Chemother. **50:**3588–3596. http://dx.doi.org/10.1128/AAC.00573-06.
17. **Neu TR, Manz B, Volke F, Dynes JJ, Hitchcock AP, Lawrence JR.** 2010. Advanced imaging techniques for assessment of structure, composition and function in biofilm systems. FEMS Microbiol. Ecol. **72:**1–21. http://dx.doi.org/10.1111/j.1574-6941.2010.00837.x.
18. **Vitkov L, Hermann A, Krautgartner WD, Herrmann M, Fuchs K, Klappacher M, Hannig M.** 2005. Chlorhexidine-induced ultrastructural alterations in oral biofilm. Microsc. Res. Tech. **68:**85–89. http://dx.doi.org/10.1002/jemt.20238.
19. **Hitchcock AP.** 2012. Soft X-ray imaging and spectromicroscopy, p 745–791. *In* Van Tendeloo G, Van Dyck D, Pennycook SJ (ed), Handbook on nanoscopy, vol II. Wiley-VCH Verlag GmbH & Co. KGaA, Weinheim, Germany.
20. **Dynes JJ, Lawrence JR, Korber DR, Swerhone GD, Leppard GG, Hitchcock AP.** 2009. Morphological and biochemical changes in *Pseudomonas fluorescens* biofilms induced by sub-inhibitory exposure to antimicrobial agents. Can. J. Microbiol. **55:**163–178. http://dx.doi.org/10.1139/W08-109.
21. **Lawrence JR, Swerhone GD, Leppard GG, Araki T, Zhang X, West MM, Hitchcock AP.** 2003. Scanning transmission X-ray, laser scanning, and transmission electron microscopy mapping of the exopolymeric matrix of

microbial biofilms. Appl. Environ. Microbiol. **69:**5543–5554. http://dx.doi.org/10.1128/AEM.69.9.5543-5554.2003.
22. **Korber DR, James GA, Costerton JW.** 1994. Evaluation of fleroxacin activity against established *Pseudomonas fluorescens* biofilms. Appl. Environ. Microbiol. **60:**1663–1669.
23. **Dynes JJ, Lawrence JR, Korber DR, Swerhone GD, Leppard GG, Hitchcock AP.** 2006. Quantitative mapping of chlorhexidine in natural river biofilms. Sci. Total Environ. **369:**369–383. http://dx.doi.org/10.1016/j.scitotenv.2006.04.033.
24. **Lawrence JR, Dynes JJ, Korber DR, Swerhone GDW, Leppard GG, Hitchcock AP.** 2012. Monitoring the fate of copper nanoparticles in river biofilms using scanning transmission X-ray microscopy (STXM). Chem. Geol. **29:**18–25. http://dx.doi.org/10.1016/j.chemgeo.2011.07.013.
25. **Liu X, Eusterhues K, Thieme J, Ciobota V, Höschen C, Mueller CW, Küsel K, Kögel-Knabner I, Rösch P, Popp J, Totsche KU.** 2013. STXM and NanoSIMS investigations on EPS fractions before and after adsorption to goethite. Environ. Sci. Technol. **47:**3158–3166. http://dx.doi.org/10.1021/es3039505.
26. **Suci PA, Vrany JD, Mittelman MW.** 1998. Investigation of interactions between antimicrobial agents and bacterial biofilms using attenuated total reflection Fourier transform infrared spectroscopy. Biomaterials **19:**327–339. http://dx.doi.org/10.1016/S0142-9612(97)00108-7.
27. **Holman HY, Miles R, Hao Z, Wozei E, Anderson LM, Yang H.** 2009. Real-time chemical imaging of bacterial activity in biofilms using open-channel microfluidics and synchrotron FTIR spectromicroscopy. Anal. Chem. **81:**8564–8570. http://dx.doi.org/10.1021/ac9015424.
28. **Suci PA, Geesey GG, Tyler BJ.** 2001. Integration of Raman microscopy, differential interference contrast microscopy, and attenuated total reflection Fourier transform infrared spectroscopy to investigate chlorhexidine spatial and temporal distribution in *Candida albicans* biofilms. J. Microbiol. Methods **46:**193–208. http://dx.doi.org/10.1016/S0167-7012(01)00268-8.
29. **Suci PA, Mittelman MW, Yu FP, Geesey GG.** 1994. Investigation of ciprofloxacin penetration into *Pseudomonas aeruginosa* biofilms. Antimicrob. Agents Chemother. **38:**2125–2133. http://dx.doi.org/10.1128/AAC.38.9.2125.
30. **Quiles F, Humbert F, Delille A.** 2010. Analysis of changes in attenuated total reflection FTIR fingerprints of *Pseudomonas fluorescens* from planktonic state to nascent biofilm state. Spectrochim. Acta A Mol. Biomol. Spectrosc. **75:**610–616. http://dx.doi.org/10.1016/j.saa.2009.11.026.
31. **Cho BJ, Lee YB.** 2002. Infectious keratitis manifesting as a white plaque on the cornea. Arch. Ophthalmol. **120:**1091–1093.
32. **del Mar Ojeda-Vargas M, Suárez-Alonso A, de Los Angeles Pérez-Cervantes M, Suárez-Gil E, Monzón-Moreno C.** 1999. Urinary tract infection associated with *Comamonas acidovorans.* Clin. Microbiol. Infect. **5:**443–444. http://dx.doi.org/10.1111/j.1469-0691.1999.tb00170.x.
33. **Horowitz H, Gilroy S, Feinstein S, Gilardi G.** 1990. Endocarditis associated with *Comamonas acidovorans.* J. Clin. Microbiol. **28:**143–145.
34. **Perla RJ, Kuntson EL.** 2005. *Delftia acidovorans* bacteremia in an intravenous drug abuser. Am. J. Infect. Dis. **1:**73–74. http://dx.doi.org/10.3844/ajidsp.2005.73.74.
35. **Mooney LD.** 2006. Triclosan's effects on natural aquatic biofilms and micro-niche biofilm formation. M. Sc. Thesis. University of Saskatchewan, Saskatoon, Saskatchewan, Canada.
36. **Hirkala DL, Germida JJ.** 2004. Field and soil microcosm studies on the survival and conjugation of a *Pseudomonas putida* strain bearing a recombinant plasmid, pADPTel. Can. J. Microbiol. **50:**595–604. http://dx.doi.org/10.1139/w04-045.
37. **Andrews JM.** 2001. Determination of minimum inhibitory concentrations. J. Antimicrob. Chemother. **48**(Suppl 1):S5–S16. http://dx.doi.org/10.1093/jac/48.suppl_1.5.
38. **Kirsop BE, Snell JSS (ed).** 1984. Maintenance of microorganisms: a manual of laboratory methods. Academic Press, London, United Kingdom.
39. **Kilcoyne AL, Tylisczak T, Steele WF, Fakra S, Hitchcock P, Franck K, Anderson E, Harteneck B, Rightor EG, Mitchell GE, Hitchcock AP, Yang L, Warwick T, Ade H.** 2003. Interferometer-controlled scanning transmission X-ray microscopes at the Advanced Light Source. J. Synchrotron. Radiation **10:**125–136. http://dx.doi.org/10.1107/S0909049502017739.
40. **Kaznatcheev KV, Karunakaran C, Lanke UD, Urquhart SG, Obst M, Hitchcock AP.** 2007. Soft X-ray spectromicroscopy beamline at the CLS: commissioning results. Nucl. Instrum. Methods Phys. Res. A **582:**96–99. http://dx.doi.org/10.1016/j.nima.2007.08.083.
41. **Dynes JJ, Tyliszczak T, Araki T, Lawrence JR, Swerhone GD, Leppard GG, Hitchcock AP.** 2006. Speciation and quantitative mapping of metal species in microbial biofilms using scanning transmission X-ray microscopy. Environ. Sci. Technol. **40:**1556–1565. http://dx.doi.org/10.1021/es0513638.
42. **Cortés ME, Sinesterra RD, Avila-Campos MJ, Tortamano N, Rocha RG.** 2001. The chlorhexidine:β-cyclodextrin inclusion compound: preparation, characterization and microbiological evaluation. J. Incl. Phenom. Macrocycl. Chem. **40:**297–302. http://dx.doi.org/10.1023/A:1012788432106.
43. **Ravaoarinoro M, Therrien C.** 1999. Beta-lactamases and outer membrane investigations in beta-lactam-resistant *Comamonas acidovorans* strains. Int. J. Antimicrob. Agents **12:**27–31. http://dx.doi.org/10.1016/S0924-8579(98)00095-8.
44. **Chotikanatis K, Bäcker M, Rosas-Garcia G, Hammerschlag MR.** 2011. Recurrent intravascular-catheter-related bacteremia caused by *Delftia acidovorans* in a hemodialysis patient. J. Clin. Microbiol. **49:**3418–3421. http://dx.doi.org/10.1128/JCM.00625-11.
45. **Stampi S, Zanetti F, Bergamaschi A, De Luca G.** 1999. *Comamonas acidovorans* contamination of dental unit waters. Lett. Appl. Microbiol. **29:**52–55. http://dx.doi.org/10.1046/j.1365-2672.1999.00575.x.
46. **Xu H, Davies J, Miao V.** 2007. Molecular characterization of class 3 integrons from *Delftia* spp. J. Bacteriol. **189:**6276–6283. http://dx.doi.org/10.1128/JB.00348-07.
47. **Valenzuela AS, Benomar N, Abriouel H, Cañamero MM, López RL, Gálvez A.** 2013. Biocide and copper tolerance in enterococci from different sources. J. Food Prot. **76:**1806–1809. http://dx.doi.org/10.4315/0362-028X.JFP-13-124.
48. **Stanley A, Wilson M, Newman HN.** 1989. The *in vitro* effects of chlorhexidine on subgingival plaque bacteria. J. Clin. Periodontol. **16:**259–264. http://dx.doi.org/10.1111/j.1600-051X.1989.tb01651.x.
49. **Wang JT, Sheng WH, Wang JL, Chen D, Chen ML, Chen YC, Chang SC.** 2008. Longitudinal analysis of chlorhexidine susceptibilities of nosocomial methicillin-resistant *Staphylococcus aureus* isolates at a teaching hospital in Taiwan. J. Antimicrob. Chemother. **62:**514–517. http://dx.doi.org/10.1093/jac/dkn208.
50. **Houari A, Di Martino P.** 2007. Effect of chlorhexidine and benzalkonium chloride on bacterial biofilm formation. Lett. Appl. Microbiol. **45:**652–656. http://dx.doi.org/10.1111/j.1472-765X.2007.02249.x.
51. **Andersson DI, Levin BR.** 1999. The biological cost of antibiotic resistance. Curr. Opin. Microbiol. **2:**489–493. http://dx.doi.org/10.1016/S1369-5274(99)00005-3.
52. **Andersson DI, Hughes D.** 2010. Antibiotic resistance and its cost: is it possible to reverse resistance? Nat. Rev. Microbiol. **8:**260–271.
53. **Björkman J, Hughes D, Andersson DI.** 1998. Virulence of antibiotic-resistant *Salmonella* Typhimurium. Proc. Natl. Acad. Sci. U. S. A. **95:**3949–3953. http://dx.doi.org/10.1073/pnas.95.7.3949.
54. **Miskinyte M, Gordo I.** 2013. Increased survival of antibiotic-resistant *Escherichia coli* inside macrophages. Antimicrob. Agents Chemother. **57:**189–195. http://dx.doi.org/10.1128/AAC.01632-12.
55. **Barrett-Bee K, Newboult L, Edwards S.** 1994. The membrane destabilising action of the antibacterial agent chlorhexidine. FEMS Microbiol. Lett. **119:**249–253. http://dx.doi.org/10.1111/j.1574-6968.1994.tb06896.x.
56. **Shen Y, Qian W, Chung C, Olsen I, Haapasalo M.** 2009. Evaluation of the effect of two chlorhexidine preparations on biofilm bacteria *in vitro*: a three-dimensional quantitative analysis. J. Endod. **35:**981–985. http://dx.doi.org/10.1016/j.joen.2009.04.030.
57. **von Ohle C, Gieseke A, Nistico L, Decker EM, DeBeer D, Stoodley P.** 2010. Real-time microsensor measurement of local metabolic activities in *ex vivo* dental biofilms exposed to sucrose and treated with chlorhexidine. Appl. Environ. Microbiol. **76:**2326–2334. http://dx.doi.org/10.1128/AEM.02090-09.
58. **Pratten J, Barnett P, Wilson M.** 1998. Composition and susceptibility to chlorhexidine of multispecies biofilms of oral bacteria. Appl. Environ. Microbiol. **64:**3515–3519.
59. **Takenaka S, Trivedi HM, Corbin A, Pitts B, Stewart PS.** 2008. Direct visualization of spatial and temporal patterns of antimicrobial action within model oral biofilms. Appl. Environ. Microbiol. **74:**1869–1875. http://dx.doi.org/10.1128/AEM.02218-07.
60. **Keren I, Kaldalu N, Spoering A, Wang Y, Lewis K.** 2004. Persister cells and tolerance to antimicrobials. FEMS Microbiol. Lett. **230:**13–18. http://dx.doi.org/10.1016/S0378-1097(03)00856-5.
61. **Castillo JA, Pinazo A, Carilla J, Infante MR, Alsina MA, Haro I, Clapés P.** 2004. Interaction of antimicrobial arginine-based cationic surfactants

with liposomes and lipid monolayers. Langmuir **20:**3379–3387. http://dx.doi.org/10.1021/la036452h.
62. **Elferink JG, Booij HL.** 1974. Interaction of chlorhexidine with yeast cells. Biochem. Pharmacol. **23:**1413–1419. http://dx.doi.org/10.1016/0006-2952(74)90361-X.
63. **Tattawasart U, Hann AC, Maillard JY, Furr JR, Russell AD.** 2000. Cytological changes in chlorhexidine-resistant isolates of *Pseudomonas stutzeri*. J. Antimicrob. Chemother. **45:**145–152. http://dx.doi.org/10.1093/jac/45.2.145.
64. **Tyler BJ, Rangaranjan S, Möller J, Beumer A, Arlinghaus HF.** 2006. TOF-SIMS imaging of chlorhexidine-digluconate transport in frozen hydrated biofilms of the fungus *Candida albicans*. Appl. Surf. Sci. **252:**6712–6715. http://dx.doi.org/10.1016/j.apsusc.2006.02.278.
65. **Richards RM, Cavill RH.** 1979. Electron-microscope study of the effect of chlorhexidine on *Pseudomonas aeruginosa*. Microbios **26:**85–93.
66. **Lieve L.** 1974. The barrier function of the gram-negative cell envelope. Ann. N. Y. Acad. Sci. **235:**109–127. http://dx.doi.org/10.1111/j.1749-6632.1974.tb43261.x.